

Retraction Notice

Title of retracted article: **Evaluation of the Impact Force of Dry Granular Flow onto Rock Shed**
 Author(s): Chun Liu, Zhixiang Yu, Junfei Huang
 * Corresponding author. Email: lc1510596295@163.com
 Journal: Journal of Geoscience and Environment Protection
 Year: 2019
 Volume: 7
 Number: 5
 Pages (from - to): 1 - 15
 DOI (to PDF): <https://doi.org/10.4236/gep.2019.75001>
 Paper ID at SCIRP: 92439
 Article page: <http://www.scirp.org/Journal/paperinformation.aspx?paperid=92439>
 Retraction date: 2019-09-16

Retraction initiative (multiple responses allowed; mark with X):

- All authors
 Some of the authors:
 Editor with hints from Journal owner (publisher)
 Institution:
 Reader:
 Other:
 Date initiative is launched: 2019-09-16

Retraction type (multiple responses allowed):

- Unreliable findings
 Lab error Inconsistent data Analytical error Biased interpretation
 Other:
 Irreproducible results
 Failure to disclose a major competing interest likely to influence interpretations or recommendations
 Unethical research
 Fraud
 Data fabrication Fake publication Other:
 Plagiarism Self plagiarism Overlap Redundant publication *
 Copyright infringement Other legal concern:
 Editorial reasons
 Handling error Unreliable review(s) Decision error Other:

Results of publication (only one response allowed):

- are still valid.
 were found to be overall invalid.

Author's conduct (only one response allowed):

- honest error
 academic misconduct
 none (not applicable in this case – e.g. in case of editorial reasons)

* Also called duplicate or repetitive publication. Definition: "Publishing or attempting to publish substantially the same work more than once."

History

Expression of Concern:

yes, date: yyyy-mm-dd

no

Correction:

yes, date: yyyy-mm-dd

no

Comment:

This article has been retracted to straighten the academic record. In making this decision the Editorial Board follows [COPE's Retraction Guidelines](#). Aim is to promote the circulation of scientific research by offering an ideal research publication platform with due consideration of internationally accepted standards on publication ethics. The Editorial Board would like to extend its sincere apologies for any inconvenience this retraction may have caused.

Evaluation of the Impact Force of Dry Granular Flow onto Rock Shed

Chun Liu, Zhixiang Yu, Junfei Huang

Department of Civil Eng., Southwest Jiaotong University, Chengdu, China

Email: lc1510596295@163.com

How to cite this paper: Liu, C., Yu, Z. X., & Huang, J. F. (2019). Evaluation of the Impact Force of Dry Granular Flow onto Rock Shed. *Journal of Geoscience and Environment Protection*, 7, 1-15.
<https://doi.org/10.4236/gep.2019.75001>

Received: December 28, 2018

Accepted: May 14, 2019

Published: May 17, 2019

Abstract

In the design of rock sheds for the mitigation of risk due to rapid and long landslides, a crucial role is played by the evaluation of the impact force exerted by the flowing mass on the rock sheds. This paper is focused on the influencing factors of the impact force of dry granular flow onto rock shed and in particular on the evaluation of the maximum impact force. The coupled DEM-FEM model calibrated with small-scale physical experiment is used to simulate the movement of dry granular flow coupled with impact forces on the rock shed. Based on the numerical results, three key stages were identified of impact process, namely startup streams slippery, impact and pile-up. The maximum impact force increases linearly with bulk density, and the maximum impact force exhibits a power law dependence on the impact height and slope angle respectively. The sensitivities of bulk density, impact height, and slope angle on the maximum impact force are: 1.0, 0.496, and 2.32 respectively in the benchmark model. The parameters with high sensitivity should be given priority in the design of the rock shed. The results obtained from this study are useful for facilitating design of shed against dry granular flow.

Keywords

Coupled DEM-FEM Method, Dry Granular Flow, Rock Shed, Impact Force, Sensitivity Analysis, Numerical Simulation

1. Introduction

The mountainous areas in Southwest China, where the topography is complex, feature seriously weathered rock masses and have experienced a large number of landslides. These landslides provide abundant materials for the initiation of dry granular flow. When the earthquake or heavy rainfall occurs, the landslide will

collide with the mountain and slide down the slope, leading to a dry granular flow (Chen & Zhang, 1994; Zhu, Wang, & Tang, 2000). The formed dry granular flow, with high speed and large displacement, can greatly threaten the safety of the residents and the smooth traffic flow. For instance, the Wenchuan earthquake caused more than 15,000 geo-hazards in the form of dry granular flows which resulted in about 20,000 deaths in 2008 (Yin, Wang, & Sun, 2009). Countermeasures have been made to minimize the dry granular flow's risk to downstream residential areas or transportation routes. There are mainly two kinds of protection structures that used to minimize this hazard: active ones (like nets) and passive ones. As active ones is hard to carry out because of avalanches' potential source area is difficult to figure out, engineers and researchers usually choose the passive ones. Rock sheds are regarded as passive protection structures and are widely used to protect against mountain hazards such as dry granular flow, due to its unique edge in terms of low construction cost and strong constructability in complex areas (Pei, Liu, & Wang, 2016; Kawahara & Muro, 2006; Mommessin, Perrotin, & Ma, 2012). Most rock sheds are made of concrete, and have a shock-absorbing layer such as sands on top of the structure (Montani, Descoedres, & Labiouse, 1996; Kishi & Konno, 2003).

Up to now, the design of such structures takes into account only the impact of an individual rock block (Kishi & Konno, 2003; Calvetti, 2011; Delhomme, Mommessin, & Mougou, 2005; Wang, Zhou, & Luo, 2017). Though the standardized design of rock sheds under a single block impact has accumulated rich engineering experience (Montani, Descoedres, & Labiouse, 1996; Kawahara & Muro, 2006), it cannot be applied to the design of rock sheds impacted by dry granular flow, due to totally different dynamic mechanical characteristics. To date, No firm guidelines built upon sounded theoretical basis are available for the design of rock shed impacted by dry granular flow. Therefore, further researches on the dynamic behavior of a rock shed impacted by a dry granular flow are urgently required. However, due to the estimation of the impact force exerted by dry granular flow is a prerequisite parameter for shed design, so it is necessary to study the influencing factors of the impact force, so as to provide references for facilitating design of shed against dry granular flow.

Physical modeling has been widely used in geotechnical engineering research because of its excellent controllability in testing conditions and good reliability of testing results. For instance, using indoor experimental methods, Jiang et al. investigated the impact of dry granular flow against a rigid retaining wall by calculating the impact force (Jiang & Towhata, 2013; Jiang, Zhao, & Towhata, 2015). Jiang designed a set of experiments to investigate the impact mechanism of dry granular flow against a curved rock shed (Jiang, Wang, & Son, 2018). Thus, the research results can serve as a significant reference for practice engineering. A quantitative analysis of impact force is eagerly needed in the design. In engineering practices, several semi-empirical methods have been used to es-

estimate the maximum impact force of debris flows acting on a rigid barrier, such as hydrostatic approach, shock wave approach and hydrodynamic approach (Shen, Zhao, & Zhao, 2018). These studies are useful for providing us with ideas. Nevertheless, these available methods still have the difficulties in estimating the impact force of dry granular flow on rock sheds. This is because each method was obtained in specific impacting and boundary conditions with strong assumptions, such that they cannot be generalized for wider applications. In addition, these methods fail to consider the influence of dry granular flow-rock shed coupled interaction. In the present study, a robust numerical tool is a good choice. As the dry granular flow is a collection composed of a large number of discrete particles, DEM is an effective method for studying dry granular flow. Lo et al. used the PFC-3D software to study the maximum impact of the rock shed suffered by the dry granular flow (Lo, Lee, & Lin, 2016). Bi et al. studied the optimization of buffer layer under the impact of dry granular flow by two-dimensional discrete element software, and obtained the optimal thickness of the buffer layer (Bi, He, & Li, 2016). However, the discrete element method is not suitable for investigations of disaster-structure coupled interaction.

The above researches generally focus on the research of a single factor of uncoupled impact force. Unfortunately, the coupled dynamic interaction between dry granular flow and a rock shed is very complicated because it depends on the kinematics of dry granular flow (like solid mass and velocity), the stiffness and geometrical characteristics of the rock shed. So a quantitative analysis of these conditions on impact force is eagerly needed in the design.

The DEM has been widely used for numerical modeling of rock avalanches (Lo, Lee, & Lin, 2016; Bi, He, & Li, 2016; Cundall, 2008). It is an appropriate tool for modeling rock avalanches because of the discrete nature of materials involved in these phenomena. On the other hand, the FEM, based on continuum mechanics theory, has been well developed. Stress-strain development path and failures of elements are easy to simulate by FEM. Therefore FEM is a highly suitable method to model the rock shed (Albaba, Lambert, & Kneib, 2017). The coupled DEM-FEM method can well consider the coupled interaction between dry granular flow-rock sheds.

In this paper, a coupled DEM-FEM method was introduced for addressing the coupled response of rock shed impacted by dry granular flow, which combines advantages of both finite element and discrete element methods (Section 2). A coupled DEM-FEM model was built. A set of spherical discrete particles were used to model the dry granular flow. The model of barrier was simulated by FEM. The numerical model was validated by comparing the numerical results with the tests (Section 3). The coupled model was naturally employed to investigate the impact process of dry granular flow on rock sheds. The model was further employed to examine the effect of bulk density of dry granular flow, impact height of dry granular flow and slope angle on the coupled impact force (Section 4).

2. Numerical Approach

2.1. DEM Modeling of Particle System

The DEM is employed to model the particle system in a dry granular flow. It is assumed that the particles are all elastic soft spheres of different sizes. The use of spherical particles in DEM simulations will inevitably lead to a soil structure different from that of real natural soils with a reduced granular internal friction. However, through careful model calibrations, an assembly of spherical particles with proper mechanical and physical properties can still be used to simulate the behavior of debris flows. This setting simplifies the complexity of dry granular flow but is also able to deliver a realistic simulation of the interaction between obstacle and flow (Bi, He, & Li, 2016; Cundall, 2008; Karajan, Han, & Teng).

2.1.1. Governing Equation

The motion of discrete elements is governed by the second Newton's law, and there are one or more forces acting on each element. The distribution and evolution of the system are described through the motion and state change of each element in the system (Cundall, 2008; Albaba, Lambert, & Kneib, 2017; Karajan, Han, & Teng, 2014). For element i :

$$\begin{cases} m_i \ddot{\mathbf{u}}_i = m_i \mathbf{g} + \sum_{k=1}^m (\mathbf{f}_{n,ik} + \mathbf{f}_{t,ik}) \\ I_i \ddot{\boldsymbol{\theta}}_i = \sum_{k=1}^m \mathbf{T}_{ik} \end{cases} \quad (1)$$

where \mathbf{g} is the gravitational acceleration. m_i , $\ddot{\mathbf{u}}_i$, I_i and $\ddot{\boldsymbol{\theta}}_i$ are the mass, translational acceleration, rotary inertia and rotational acceleration of element i respectively. $\mathbf{f}_{n,ik}$, $\mathbf{f}_{t,ik}$ and \mathbf{T}_{ik} are the normal contact force, the tangential contact force and the torques of element i acted by its neighboring element k respectively. \mathbf{T}_{ik} can be obtained by formula $\mathbf{T}_{ik} = \mathbf{l}_{ik} \times (\mathbf{f}_{n,ik} + \mathbf{f}_{t,ik})$, and \mathbf{l}_{ik} is the arm vector of the force to the center of element i .

2.1.2. Evaluation of Contact Forces

Particles in the simulations are interacting with a linear spring-dashpot contact (LSD) law with Coulomb failure criterion, which is simple and computationally efficient compared to Hertz contact model (Karajan, Han, & Teng, 2014). The contact model of two particles is shown in **Figure 1**.

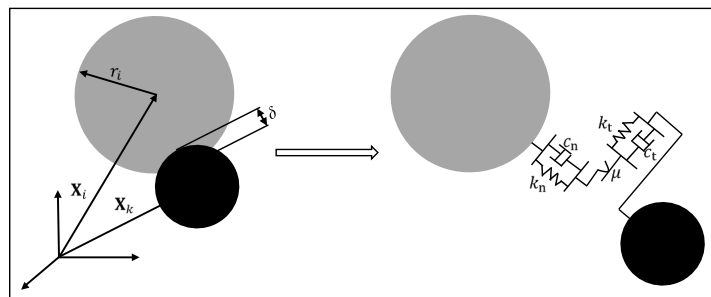


Figure 1. Contact model of two particles.

The overlap δ of two particles is calculated as follows:

$$\delta = r_i + r_k - |\mathbf{x}_i - \mathbf{x}_k| \quad (2)$$

where r_i and r_k are the radius of particles i and k respectively. \mathbf{x}_i and \mathbf{x}_k are the position vector of particles i and k respectively.

The normal contact force $\mathbf{f}_{n,ik}$ between interacting particles is calculated as follows:

$$\mathbf{f}_{n,ik} = (-k_n \delta + c_n \dot{\delta}) \mathbf{n} \quad (3)$$

where k_n , c_n , $\dot{\delta}$, and \mathbf{n} are the normal spring stiffness, normal damping coefficient, the relative normal velocity and the unit normal displacement vector respectively.

The tangential contact forces $\mathbf{f}_{t,ik}$ between interacting particles are calculated as follows:

$$\mathbf{f}_{t,ik} = \begin{cases} (-k_t \delta_t + c_t \dot{\delta}_t); & \text{if } |\mathbf{f}_{n,ik}| \mu > |-k_n \delta_t + c_t \dot{\delta}_t| \\ \sum_{k=1}^m \mathbf{T}_{ik} \frac{(-k_t \delta_t + c_t \dot{\delta}_t)}{|-k_t \delta_t + c_t \dot{\delta}_t|} |\mathbf{f}_{n,ik}| \mu; & \text{otherwise} \end{cases} \quad (4)$$

where k_t , c_t , δ_t and μ are the tangential spring stiffness, tangential damping coefficient, the incremental tangential displacement, and the friction coefficient respectively. k_t is taken as $2/7 k_n$ (Albaba, Lambert, & Kneib, 2017; Karajan, Han, & Teng, 2014). k_n is calculated as follows (Karajan, Han, & Teng, 2014):

$$\kappa_n = \eta_n \frac{\kappa_i r_i \kappa_k r_k}{\kappa_i r_i + \kappa_k r_k}, \quad \text{and } \kappa = \frac{E}{3(1-2\nu)} \quad (5)$$

where η_n is a stiffness proportionality constant. κ_i and κ_k are the bulk modulus of particle i and k respectively. E and ν are the elastic modulus and poisson ratio of particle respectively.

c_n and c_t are calculated as follows (Karajan, Han, & Teng, 2014):

$$c_n = 2\eta_n \sqrt{\frac{m_i m_k}{m_i + m_k}} k_t, \quad c_t = 2\eta_t \sqrt{\frac{m_i m_k}{m_i + m_k}} k_n \quad (6)$$

where η_n and η_t are the normal damping ratio and tangential damping ratio of particles respectively.

2.2. Coupled DEM-FEM Model

The coupled governing equations are given by Equation (7). The first and second conditions refer to the governing equations of DEM. The final condition gives the governing equation of FEM.

$$\begin{cases} m_i \ddot{\mathbf{u}}_i = m_i \mathbf{g} + \sum_{k=1}^m (\mathbf{f}_{n,ik} + \mathbf{f}_{t,ik}) + \sum_{j=1}^l (\mathbf{f}_{n,ij} + \mathbf{f}_{t,ij}) \\ I_i \ddot{\boldsymbol{\theta}}_i = \sum_{k=1}^m \mathbf{T}_{ik} + \sum_{j=1}^l \mathbf{T}_{ij} \\ M \ddot{\mathbf{X}} + C \dot{\mathbf{X}} + K \mathbf{X} = \mathbf{f}_a + \mathbf{f}_b \end{cases} \quad (7)$$

where $\mathbf{f}_{n,ij}$, $\mathbf{f}_{t,ij}$ and \mathbf{T}_{ij} are the normal contact force, tangential contact force and the torques of discrete element i acted by its neighboring finite element j respectively. \mathbf{T}_{ij} can be obtained by formula $\mathbf{T}_{ij} = \mathbf{I}_{ij} \times (\mathbf{f}_{n,ij} + \mathbf{f}_{t,ij})$, and \mathbf{I}_{ij} is the arm vector of the force. M , C , and K are the mass matrix, damping matrix and stiffness matrix of system respectively. \mathbf{X} is the displacement of finite element node. \mathbf{f}_a and \mathbf{f}_b are the external force vector of finite elements and the contact force vector of between finite elements and discrete elements respectively.

The interaction between contact surfaces is handled following the penalty method. As before-mentioned, the combined finite-discrete element method proposed in this paper is focused at dynamic simulation, and the Central Difference Method (CDM) is employed to solve Equation (7). Since CDM is conditional convergence, the step must satisfy the numerical stability conditions. Both DEM and FEM adopt the conditional stable central difference method, and their coupling requires that their integrals must be synchronized, which requires both to adopt the same time step under the same calculation framework. The time step $\Delta t_{\text{DEM-FEM}}$ takes the smaller value of both (Karajan, Han, & Teng, 2014).

$$\Delta t_{\text{DEM-FEM}} = \min(\Delta t_{\text{DEM}}, \Delta t_{\text{FEM}}) \quad (8)$$

where $\Delta t_{\text{DEM}} = \beta 0.2\pi \sqrt{m/K_{\text{spring}}}$ and $\Delta t_{\text{FEM}} \leq L_{\text{min}}/c$. c is the material sound speed. β is the scaling coefficient of time step length. m is the particle mass. K_{spring} is the contact spring stiffness of particles, and L_{min} is the minimum finite element size.

3. Verification of Coupled DEM-FEM Model

3.1. Experimental Model

The flume, which measured 2.93 m in length, 0.35 m in height, and 0.3 m in width, was constructed to reproduce the flow environment of dry particles as shown in Figure 2. The side walls of the flume were covered by 1 mm thick

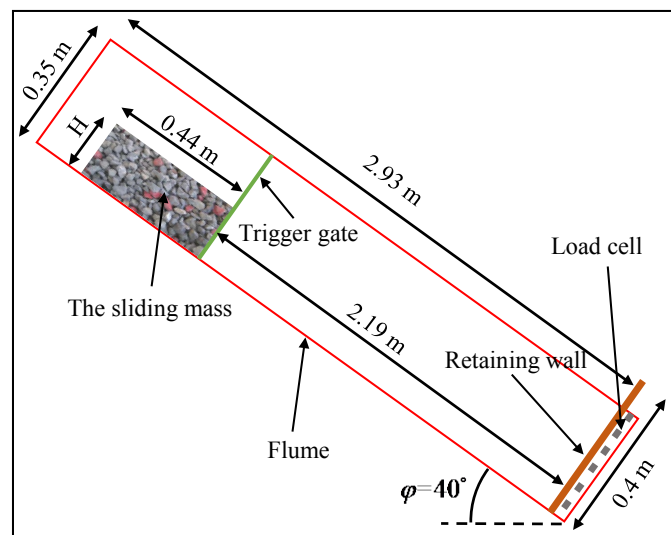


Figure 2. Sketch of the experimental flume.

polyethylene sheets for protection. The base of the flume was covered by a type of acrylic board to produce base friction. A retaining wall instrumented with 6 load cells was installed at the bottom end of the flume, perpendicular to the flume base, and the impact force in the normal direction was measured. The summation of these six force fractions of the load cells is the total force exerted on the retaining wall. A trigger gate was used to instigate the flow of the sliding mass. The length of the initial deposition of the sliding mass is 0.44 m. The height H of the initial deposition is 0.15 m. The distance between the trigger gate and the retaining wall model is 2.19 m. The width of retaining wall is 300 mm, the same as that of the flume. The tilt angle of the flume is 40° . The particle sizes range from 10 mm to 25 mm. The specific parameters are shown in **Table 1** (Jiang & Towhata, 2013).

3.2. Numerical Model

Due to the existence of inter-particle porosity, the density of sand is set to 2800 kg/m^3 through the numerical volume test (Adrian Jensen, Kirk Fraser & George Laird, 2014), so that the bulk density of the initial debris deposition could be guaranteed to be 1350 kg/m^3 . This test allows the analyst to adjust the bulk density. The normal damping ratio between particles is set to 0.7. The tangential damping ratio is set to 0.4. The stiffness proportionality constant is set to 0.01. These three values were obtained by trial and error, so that the overall numerical results of debris dynamics can match the experimental observations in the model validation process. The particle Young's modulus and Poisson's ratio are set according to the commonly used values in numerical simulations of granular medium, as listed in **Table 2**. The initial debris deposition is composed of an assembly of 4968 randomly distributed spherical particles.

As a channel, the side wall and bottom wall have little influence on the test, and so they are modeled as rigid wall. In the experiment, the load cells upon impact have a very small normal strain, and so the retaining wall is simulated by elastic wall. The material parameters are shown in **Table 2**. All the walls are simulated with 4-node thin-shell elements, and the mesh size is 0.01 m.

The friction coefficients of the particles (μ_1), the flume base (μ_2) and the barrier (μ_3) are chosen according to the experimental observations (Jiang YJ & Towhata I, 2013). In all the simulations, the flow is initiated by instantaneous removal of the top trigger gate. Then, the granular mass would slide under gravity downwards the flume with confined motions by the two side walls. At the bottom end of the flume, the granular mass is arrested by the barrier.

Table 1. Material properties of dry particles.

Dry bulk density	1350 kg/m^3	Angle of repose	53°
D_{50}	14.1 mm	Friction angle of side wall-particles	25°
Uniformity coefficient, C_u	1.5	Friction angle of bottom wall-particles	21°
		Friction angle of retaining wall-particles	15°

Table 2. Model parameters adopted for the coupled DEM-FEM simulations.

	Density	2800 kg/m ³		Density	2000 kg/m ³
	Young's modulus	30 Gpa	Wall (Rigid)	Young's modulus	30 Gpa
	Poisson's ratio	0.3		Poisson's ratio	0.3
	Normal damping ratio	0.7		Density	7850 kg/m ³
Granular	Tangential damping ratio	0.4	Barrier (Elastic)	Young's modulus	200 Gpa
	Stiffness proportionality constant	0.01		Poisson's ratio	0.3
	Particle-particle friction coefficient μ_1	1.38			
	particle-flume friction coefficient μ_2	0.47	Gravitational acceleration		9.8 m/s ²
	particle-barrier friction coefficient μ_3	0.38			

3.3. Model Validation

It can be observed that the numerical results can match well the experimental measurements (see **Figure 3**). Both of them are very similar in granular deposition shape, the length error of the granular deposition shape along the bottom direction of the sand trough is 14.3%, and the length error of the granular deposition shape along the height direction of the barrier baffle is 10%. A static pressure dead zone is formed at the baffle (see **Figure 3(a)**). In particular, it is apparent that the numerical simulation result can represent the general trend of the impact force evolution. The maximum impact force of test and simulation is 788.6 N and 824.4 N respectively, and the error is no more than 4.54% (see **Figure 3(b)**). The numerical simulation can capture the characteristics of the peak force observed in experiments.

4. Parametric Study

A comparison between the experimental and the numerical results indicates that the coupled DEM-FEM experiment adopted in this study can well simulate the

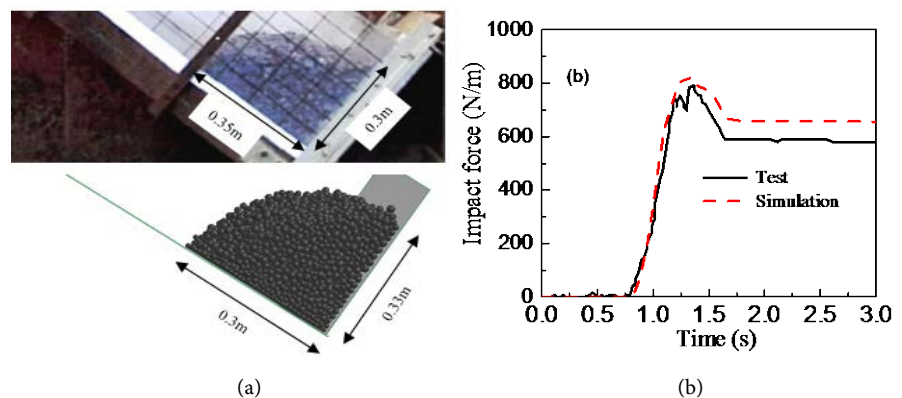


Figure 3. Comparison of test and simulation results: (a) granular deposition shape; (b) time history curves of impact force.

laboratory experiment. In this paper, based on the indoor model of dry granular flow against a retaining wall, a model of rock shed impacted by a dry granular flow is established by placing the retaining wall at the horizontal plane. Moreover, it is advisable to implement a numerical experiment for investigation of influencing factors of the avalanche-structure interaction.

4.1. Problem Geometry and Numerical Model

The model of rock shed impacted by a dry granular flow is established by placing the retaining wall at the horizontal plane. For the simplified model, the rectangularly shaped debris flow material may not have the same impact energy compared with the actual case; however, this paper aims to study the regular variation of impact energy for qualitative analysis rather than quantitative examination. Simplifying the model makes the analysis simpler and easier. The geometric scheme adopted for this study is shown in Figure 4, which identifies the key parameters, including the bulk density of dry granular flow (ρ), impact height of dry granular flow (H) and slope angle (θ). In Table 3, numerical values are assigned to all geometric parameters used here. In this study, the scale shed model aims to quantitatively study the variation of impact force with these key parameters. Because this paper aims to study the forces on the slab of the shed structure, only the slab is taken for coupled analysis. The slab is fixed with four corners. The slab here is simulated with elastic shell elements. Their material parameters

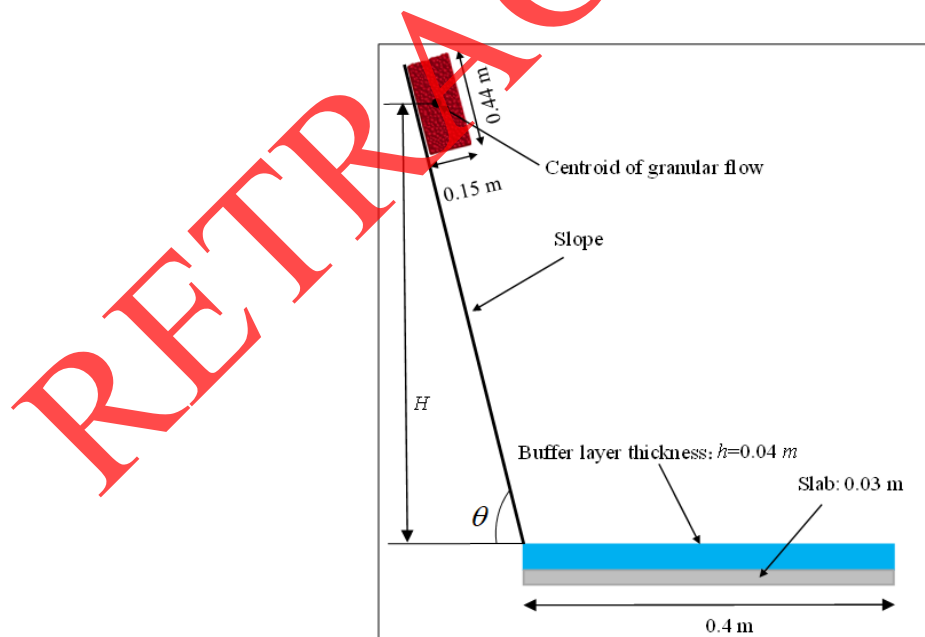


Figure 4. Sketch model of rock shed.

Table 3. The main parameters used in the parametric studies.

ρ (kg/m ³)	1060, 1205, 1350, 1495, 1640	$H = 3.0$ m, $\theta = 60^\circ$
H (m)	2.0, 2.5, 3.0, 3.5, 4.0	$\rho = 1350$ kg/m ³ , $\theta = 60^\circ$
θ (°)	44, 52, 60, 68, 76	$\rho = 1350$ kg/m ³ , $H = 3.0$ m

are shown in **Table 2**. The buffer layer covering the slab is composed of gravel cushion layer. The gravel parameter studies using DEM have been extensively conducted by many scholars (Chaplot, Walter, & Curmi, 2000; Takahara & Miura, 1998). Takahara et al. used the DEM to simulate the gravel material and found that DEM reflected the physical properties better (Takahara & Miura, 1998). In this paper, the particle diameter is randomly and uniformly set as 8 - 10 mm. For convenience, other material parameters are the same as dry granular flow.

4.2. Impact Process

In this section, the general features of granular flow impacting on a rock shed of $\rho = 1350 \text{ kg/m}^3$, $H = 2.5 \text{ m}$ and $\theta = 60^\circ$ are illustrated. **Figure 5** shows the evolution of granular profiles during the impacting process. Based on the numerical results, the evolutions of granular flow deposition can be divided into three key stages, namely the startup streams slippery, impact and pile-up. In the startup streams slippery stage (0 - 0.78 s), it can be observed that, with the increase of time, the speed difference between front and tail increases. The granular flow consists of three parts: front, middle and tail, and the flow pattern of granular flow is basically formed. When $t = 0.78 \text{ s}$, the velocities of the three parts of the particle flow are 6.4 m/s, 3.8 m/s and 2.6 m/s in the front, middle and tail respectively. In the impact stage (0.78 - 1.1 s), it can be observed that, the cushion layer is highly deformed. The buffer layer dissipates the kinetic energy of the granular flow and reduces the impact force. In the pile-up stage (0.78 - 1.1 s), the granular flow particles begin to slow down, and the shape of the granular flow becomes gradually convex with respect to the shedslab. The final deposition is shown in **Figure 5** ($t = 3.0 \text{ s}$). Only a small portion of the granular flows stays on the shed slab, and most of them will eventually accumulate on the ground after sliding out of the shedslab. The granular flow is basically in a stable state and accumulates in the dead zone, which can act as a buffer layer against the next flow shock.

4.3. Impact Force Results

Figure 6 shows the effect of bulk density on impact force. It can be seen from **Figure 6(a)** that particles of different densities reach their maximum impact force at almost the same time, and the whole impact process last about 0.5 s. **Figure 6(b)** gives a strong linear correlation between maximum impact force and bulk density. A popular formula for estimation of the maximum impact force is based on the well-known hydrodynamic model which shows a positive linear correlation between the maximum impact force and the density (Kwan, 2012). This also indicates the common character of granular impact: the maximum impact force has a strong linear correlation with the bulk density.

Figure 7 shows the effect of impact height on impact force. As shown in **Figure 7(a)**, the maximum impact force increases with the increase of impact height. Because of the increasing of the impact height, the gravitational potential

energy of dry granular flow increases, leading to the increasing of the velocity of the dry granular flow front. **Figure 7(b)** gives a strong power function correlation between the maximum impact force and the impact height. The rate of increment about the maximum force declines as the impact height ascends.

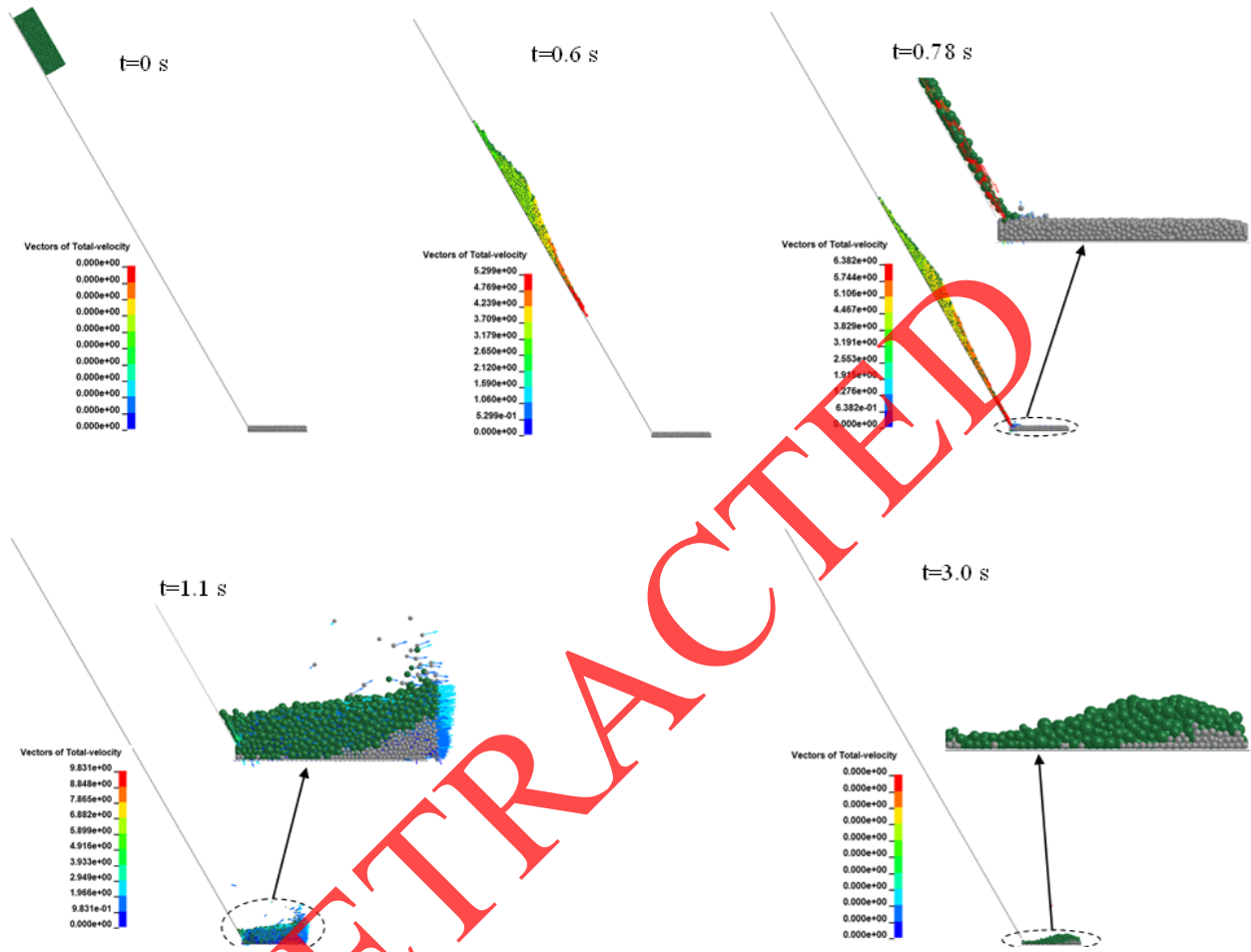


Figure 5. Evolution of dry granular flow motions during the impact against a rock shed.

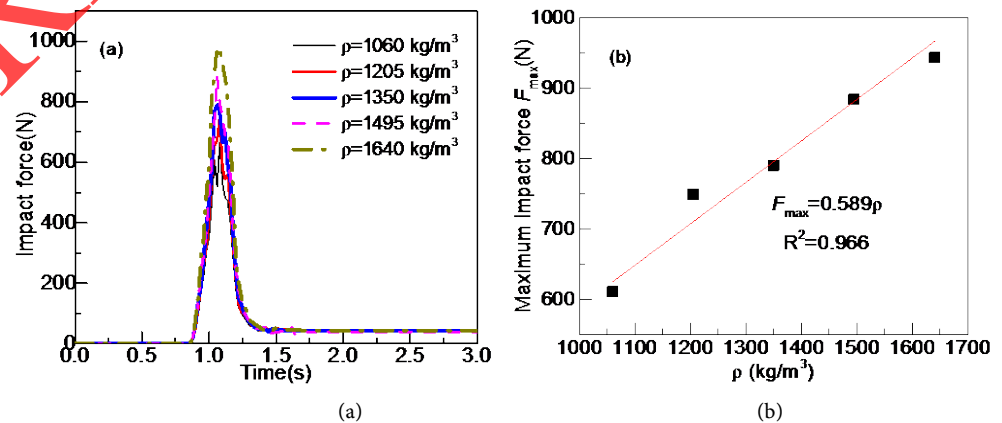


Figure 6. Effect of density on impact force: (a) the impact force evolution with time and (b) the relationship between maximum impact force and bulk density.

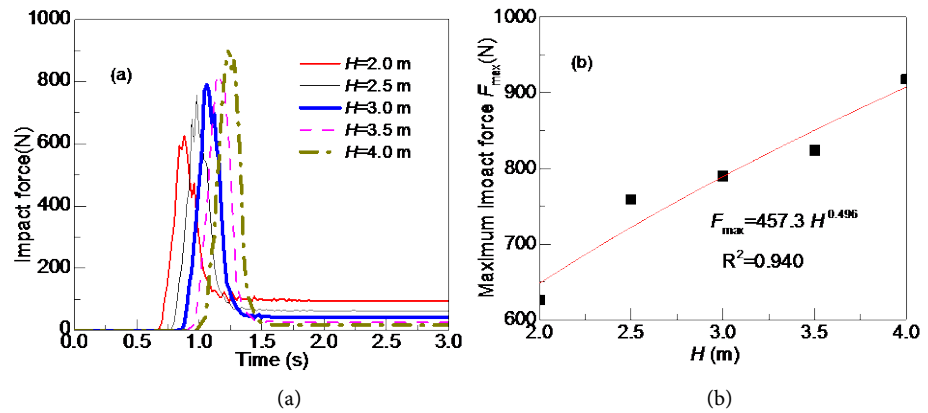


Figure 7. Effect of impact height on impact force: (a) the impact force evolution with time and (b) the relationship between maximum impact force and impact height.

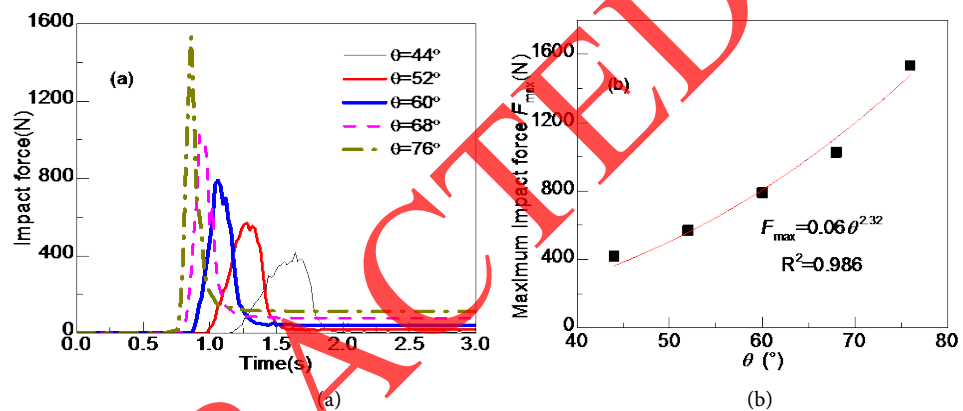


Figure 8. Effect of slope angle on impact force: (a) the impact force evolution with time and (b) the relationship between maximum impact force and slope angle.

Figure 8 shows the effect of slope angle on impact force. As shown in **Figure 8(a)**, as the slope angle increases, the maximum impact force increases and the impact duration decreases. This is because under the same impact height, the overall potential energy of the dry granular flow is the same. The larger slope angle, the smaller the velocity difference between the front and tail, the shorter flow length of the flow, and the larger average flow depth. On the other hand, with the increasing of slope angle, the friction energy consumption reduces and the front velocity of the flow increases, leading to the greater impact force at the shed slab. **Figure 8(b)** gives a strong power function correlation between maximum impact force and slope angle. The rate of increment about the maximum force ascends as the slope angle ascends.

4.4. Sensitivity Analysis

The sensitivity analysis method in the system analysis can be used to determine the main influence parameters. The relationship between the parameters of the dry granular flow and the maximum impact force is respectively fitted, and Equation (9) is obtained.

$$\begin{cases} F_{\max} = 0.589\rho; R^2 = 0.966 \\ F_{\max} = 457.3H^{0.496}; R^2 = 0.940 \\ F_{\max} = 0.06\theta^{2.32}; R^2 = 0.986 \end{cases} \quad (9)$$

According to the sensitivity calculation formula 10 (Zhang & Zhun, 1993):

$$S_{a_k}^* = \left| \left(\frac{d\varphi_k(a_k)}{da_k} \right)_{a_k=a_k^*} \right| \frac{a_k^*}{U^*} \quad (10)$$

where $S_{a_k}^*$ is sensitivity value. $\varphi_k(a_k)$ is the sensitivity function of sensitivity parameter a_k , which is the fitting function in this paper. a_k^* is the reference value of sensitivity parameters. U^* is the value of sensitivity function when $a_k = a_k^*$.

The reference values of parameters of the benchmark model for sensitivity analysis in this paper are: $\rho_0 = 1350 \text{ kg/m}^3$, $H_0 = 3.0 \text{ m}$ and $\theta_0 = 60^\circ$. The corresponding maximum impact force $F_{\max,0}$ is 790 N. Through Equation (10), the sensitivity value of each parameter in the benchmark model is shown in **Table 4**. The most important factor affecting the maximum impact force is slope angle, followed by bulk density, and the impact height has the least effect on the maximum impact force. The parameters with higher sensitivity value should be considered in the rock shed design.

5. Conclusion and Discussion

The impact of a dry granular flow on a rock shed has been investigated by a novel numerical framework. A coupled DEM-FEM approach is employed in this framework. The coupled DEM-FEM model was successfully verified by indoor test results. As such, the validated model was then employed to investigate the evaluation of the maximum impact force of dry granular flow against rock shed under different influencing factors. The key findings from this study are summarized as follows:

Based on the numerical modeling, three key stages during impact process, namely the startup streams slippery, impact and pile-up were identified.

Certain outcomes were discussed with particular emphasis on the influences of bulk density, impact height, and slope angle on the impact forces exerted on the rock shed. The maximum impact force increases linearly with bulk density. The maximum impact force increases in the form of a power law with the increases of the impact height, and its power index is less than 1. The maximum impact force increases in the form of a power law with the increases of the slope angle, and the power index is greater than 1. The sensitivities of bulk density, impact height, and slope angle on the maximum impact force are: 1.0, 0.496,

Table 4. Sensitivity of the parameters of the benchmarking model.

Sensitive parameters	S_ρ^*	S_H^*	S_θ^*
Sensitivity value	1.01	0.49	2.36

and 2.32 respectively in the benchmark model. The parameters with high sensitivity should be given priority in the design of the rock shed.

However, this paper remains a rather preliminary pilot study. Only the maximum impact force of the dry granular flow on the rock shed is taken as the dependent variable, and the response to the internal force of rock shed needs to be further modeled and analyzed. On the other hand, the effects of the buffer layer and initial shape of granular flow on the maximum impact force need to be further study.

Acknowledgements

This research was supported by the National Natural Science Foundation of China under Grant No. 51678504 and No. 51408498.

Conflicts of Interest

The authors declare no conflicts of interest regarding this article.

References

- Albaba, A., Lambert, S., Kneib, F. et al. (2017). DEM Modeling of a Flexible Barrier Impacted by a Dry Granular Flow. *Rock Mechanics & Rock Engineering*, 50, 3029-3048. <https://doi.org/10.1007/s00603-017-1286-z>
- Bi, Y.-Z. He, S.-M., Li, X.-P. et al. (2016). Geo-Engineered Buffer Capacity of Two-Layered Absorbing System under the Impact of Rock Avalanches Based on Discrete Element Method. *J. Mt. Sci.*, 13, 917-929. <https://doi.org/10.1007/s11629-014-3354-0>
- Calvetti, F. (2011). Rockfall Shelters Covered by Granular Layers: Experiments and Design Approach. *European Journal of Environmental and Civil Engineering*, 15, 73-100. <https://doi.org/10.1080/19648189.2011.9695305>
- Chaplot, V., Walter, C., & Curmi, P. (2000). Improving Soil Hydromorphy Prediction According to DEM Resolution and Available Pedological Data. *Geoderma*, 97, 405-422. [https://doi.org/10.1016/S0016-7061\(00\)00048-3](https://doi.org/10.1016/S0016-7061(00)00048-3)
- Chen, Z. S., & Zhang, X. G. (1994). A Hazardchain of Landslide→Collapse→Debris Flow→River Stoppage in Wulong County, Sichuan Province on April 30, 1994. *Mountain Research*, 12, 225-229.
- Cundall, P. A. (2008). A Discrete Numerical Model for Granular Assemblies, Numerical Model for Granular Assemblies. *Geotechnique*, 29, 331-336.
- Delhomme, F., Mommessin, M., Mougoin, J. P. et al. (2005). Behavior of a Structurally Dissipating Rock-Shed: Experimental Analysis and Study of Punching Effects. *International Journal of Solids & Structures*, 42, 4204-4219. <https://doi.org/10.1016/j.ijsolstr.2004.12.008>
- Jensen, A., Fraser, K., & Laird, G. (2014). Improving the Precision of Discrete Element Simulations through Calibration Models. *13th International LS-DYNA Users Conference*.
- Jiang, Y. J., & Towhata, I. (2013). Experimental Study of Dry Granular Flow and Impact Behavior against a Rigid Retaining Wall. *Rock Mech Rock Eng*, 46, 713-729. <https://doi.org/10.1007/s00603-012-0293-3>
- Jiang, Y. J., Wang, Z. Z., Song, Y. et al. (2018). Cushion Layer Effect on the Impact of a Dry Granular Flow against a Curved Rock Shed. *Rock Mechanics & Rock Engineering*,

51, 2191-2205. <https://doi.org/10.1007/s00603-018-1478-1>

Jiang, Y. J., Zhao, Y., Towhata, I. et al. (2015). Influence of Particle Characteristics on Impact Event of Dry Granular Flow. *Powder Technol*, 270, 53-67.

<https://doi.org/10.1016/j.powtec.2014.10.005>

Karajan, N., Han, Z., Teng, H. et al. (2014). On the Parameter Estimation for the Discrete-Element Method in LS-DYNA. *13th International LS-DYNA User Conference*.

Kawahara, S., & Muro, T. (2006). Effects of Dry Density and Thickness of Sandy Soil on Impact Response Due to Rockfall. *Journal of Terramechanics*, 43, 329-340.

<https://doi.org/10.1016/j.jterra.2005.05.009>

Kishi, N., & Konno, H. (2003). Numerical Analysis Model for Three Layer Absorbing System under Falling Weight Impact Loading. *JSCCE Journal of Structural Engineering*, 49, 1323-1332.

Kwan, J. S. H. (2012). *Supplementary Technical Guidance on Design of Rigid Debris-Resisting Barriers*. Technical Note No.TN 2/2012. Geotech. Eng. Off (Civil Engineering and Development Department, The HKSAR Government).

Lo, C.-M., Lee, C.-F., & Lin, M.-L. (2016). Consideration of the Maximum Impact Force Design for the Rock-Shed Slab. *Journal of Geography & Natural Disasters*, 6.

<https://doi.org/10.4172/2167-0587.1000169>

Mommessin, M., Perrotin, P., & Ma, Y. (2012). Actions of Snow Avalanches on a Protection Gallery. *Cold Regions Science and Technology*, 83, 20-29.

<https://doi.org/10.1016/j.coldregions.2012.05.015>

Montani, S., Descoeurdes, F., & Labiouse, V. (1996). Experimental Study of Rock Sheds Impacted by Rock Blocks. *Structural Engineering International*, 6, 171-175.

<https://doi.org/10.2749/101686696780495536>

Pei, X.-J., Liu, Y., & Wang, D.-P. (2016). Study on the Energy Dissipation of Sandy Soil Cushions on the Rock-Shed under Rockfall Impact Load. *Journal of Sichuan University (Engineering Science Edition)*, 48, 15-22.

Shen, W., Zhao, T., Zhao, J. et al. (2018). Quantifying the Impact of Dry Debris Flow against a Rigid Barrier by DEM Analyses. *Engineering Geology*, 241, 86-96.

<https://doi.org/10.1016/j.enggeo.2018.05.011>

Takahara, T., & Miura, K. (1998). Mechanical Characteristics of EPS Block Fill and Its Simulation by DEM and FEM. *Soils and Foundations*, 38, 97-110.

Wang, S., Zhou, X.-J., Luo, F.-J. et al. (2017). An Experimental Study on the Performance of an Arch Shaped Rock Shed Due to the Impact of Rockfall. *Journal of Vibration and Shock*, 36, 215-222.

Yin, Y., Wang, F., & Sun, P. (2009). Landslide Hazards Triggered by the 2008 Wenchuan Earthquake, Sichuan, China. *Landslides*, 6, 139-152.

<https://doi.org/10.1007/s10346-009-0148-5>

Zhang, G., & Zhun, W. S. (1993). Parameter Sensitivity Analysis and Test Scheme Optimization. *Rock and Soil Mechanics*, 51-58.

Zhu, P. Y., Wang, C. H., & Tang, B. X. (2000). The Deposition Characteristic of Supper Debris Flow in Tibet. *Journal of Mountain Science*, 18, 453-456.